

An efficient quantum algorithm for the time evolution of parameterized circuits

Stefano Barison, Filippo Vicentini, and Giuseppe Carleo

Institute of Physics, École Polytechnique Fédérale de Lausanne (EPFL), CH-1015 Lausanne, Switzerland

We introduce a novel hybrid algorithm to simulate the real-time evolution of quantum systems using parameterized quantum circuits. The method, named "projected - Variational Quantum Dynamics" (p-VQD) realizes an iterative, global projection of the exact time evolution onto the parameterized manifold. In the small time-step limit, this is equivalent to the McLachlan's variational principle. Our approach is efficient in the sense that it exhibits an optimal linear scaling with the total number of variational parameters. Furthermore, it is global in the sense that it uses the variational principle to optimize all parameters at once. The global nature of our approach then significantly extends the scope of existing efficient variational methods, that instead typically rely on the iterative optimization of a restricted subset of variational parameters. Through numerical experiments, we also show that our approach is particularly advantageous over existing global optimization algorithms based on the time-dependent variational principle that, due to a demanding quadratic scaling with parameter numbers, are unsuitable for large parameterized quantum circuits.

I. INTRODUCTION

In recent years, our ability to manipulate and measure quantum systems has improved tremendously. Among all experimental platforms, the number of addressable qubits has increased remarkably: both Google [1] and IBM [2] have reported superconducting circuits chips with ≈ 50 qubits and according to their public timelines they expect to build 1000-qubit devices within the next 2 years. Despite this impressive development, universal quantum-computing remains still far in the future. Algorithms such as Shor's [3], Quantum-Fourier Transform [4] or general Quantum Simulators [5–7] require a number of operations (gates) at least polynomial in the qubit number. However, in the absence of large-scale quantum error correction, the number of gates that can be applied is at present strongly limited by hardware noise and decoherence.

To circumvent the problem, current generations of quantum algorithms rely on a hybrid classical-quantum approach [8–12]. A typical example is given by the classical optimization of a quantum circuit encoding the solution of a given problem. Quantum circuits can be used as the model of a machine-learning problem [13, 14], such as a quantum classifiers [15, 16], quantum kernel machines [17–19], quantum Boltzmann machines [20] or convolutional networks [21] to name a few. Quantum circuits can also be used to directly approximate the state of an interacting quantum system [22–24]. In particular, several of the proposed hybrid algorithms extend the use of the variational method to quantum computing: a trial quantum state (ansatz state) with a tractable number of parameters and mild circuit depth is considered, then these parameters are optimized in order to approximate a target state as accurately as possible.

For quantum simulation, a variational, resource friendly alternative to Trotterization [25–28], has been introduced in 2017 [9, 29]. This algorithm is based on a reformulation of the Dirac-Frenkel and McLachlan variational principle [30–32], called the time-dependent variational

principle. The Time-Dependent Variational Algorithm (TDVA) encodes the state into a variational circuit and iteratively updates the parameters by solving a Euler-Lagrange equation of motion. The computational cost of this approach is dominated by the stochastic estimation of the Quantum Geometric Tensor [33, 34] and its inversion, resulting in an expensive quadratic cost in the total number of variational parameters. To alleviate this issue, new variational methods based on partial, local optimisations of the variational parameters have been recently proposed. These are hardware efficient [35] or inspired by classical tensor-network optimization approaches [36].

In this paper we propose an hybrid quantum algorithm for approximating the real time evolution of an interacting quantum system, called projected-Variational Quantum Dynamics (p-VQD). This algorithm overcomes the drawbacks of existing approaches in that it is both global – it optimizes all parameters at once – and efficient – it scales linearly with the number of parameters. Moreover, it does not require auxiliary (ancilla) qubits and the depth of the circuit is constant throughout all the simulation. The structure of this paper is as follows: in Section II we present the algorithm in order to simulate real time evolution of quantum systems, while in Section III we benchmark our algorithm on a Transverse Field Ising model, assessing the accuracy of the method on an ideal quantum simulator performing single and multi shot executions. We conclude, in Section IV, with some considerations on the proposed algorithm.

II. METHOD

We address the simulation of a quantum system with Hamiltonian \hat{H} . For clarity of exposition we will assume that \hat{H} is time independent, but it is not a requirement of the algorithm. The time evolution operator for a small time-step $\delta t \in \mathbf{R}$ is $e^{-i\hat{H}\delta t}$. Let $|\psi_{w(t)}\rangle$ be the parametrized ansatz state approximating the exact quantum state of the system $|\Psi(t)\rangle$ at time t , where

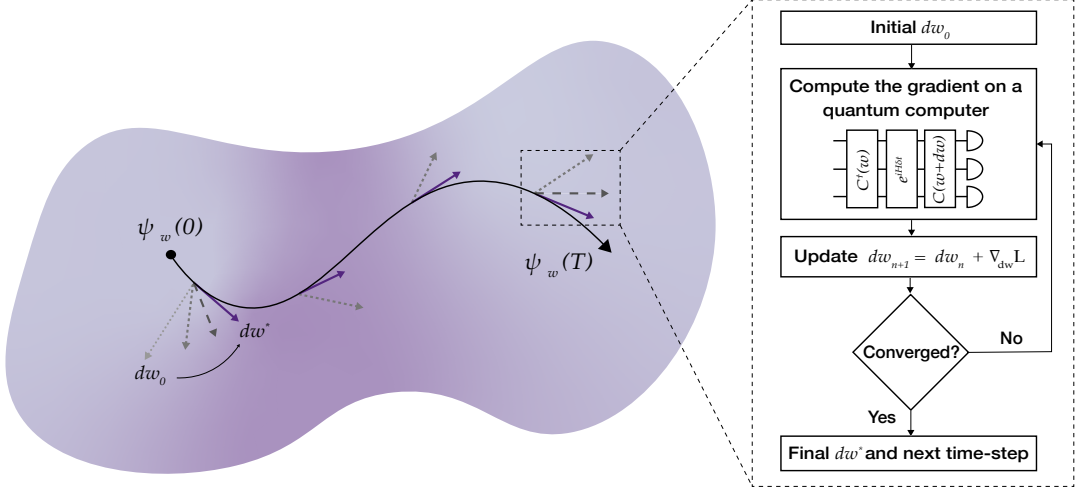


Figure 1. Sketch of the p-VQD algorithm. We follow the real time evolution of the ansatz state $\psi_w(t)$ in the Hilbert space by optimizing the parameter variation dw at every time step. The optimization is performed through the gradient of the step-infidelity function $L(dw, \delta t)$, computed using a quantum computer.

$w(t) \in \mathbf{R}^p$ is the vector of its p -parameters. We assume $|\psi_w(t)\rangle$ is a unit vector and define the evolved state $|\phi(t + \delta t)\rangle = e^{-iH\delta t}|\psi_w(t)\rangle$. From now on, we will indicate $w(t)$ as w to simplify the notation, implying that the parameters we are referring to are the one assigned to the ansatz at time t , except when explicitly indicated. Also the notation of $|\phi(t + \delta t)\rangle$ will be simplified to $|\phi(\delta t)\rangle$.

In order to variationally approximate the time evolution of the system, we aim to maximize the overlap between the evolved parametrized state $|\phi(\delta t)\rangle$ and the state $|\psi_{w+dw}\rangle$, where $dw \in \mathbf{R}^p$ is a vector of parameter variations. We want to find dw such that

$$\arg \max_{dw \in \mathbf{R}^p} |\langle \phi(\delta t) | \psi_{w+dw} \rangle|^2. \quad (1)$$

Similarly to [37], we derive the condition indicated in Eq. (1) defining the projected real-time evolution, as can be seen in Appendix A. The optimal update dw^* therefore minimizes the step-infidelity

$$L(dw, \delta t) = \frac{1 - |\langle \phi(\delta t) | \psi_{w+dw} \rangle|^2}{\delta t^2}, \quad (2)$$

where the $\frac{1}{\delta t^2}$ factor has been added to make L independent from the time-step size in the limit of $\delta t \rightarrow 0$. More details about the introduction of this factor can be found in Appendix B. Given that the wavefunction is encoded as the circuit $C(w)$, substituting into the loss function in Eq. (2) the definition $|\psi_w\rangle = C(w)|0\rangle$ we obtain,

$$L(dw, \delta t) = \frac{1 - |\langle 0 | C^\dagger(w) e^{iH\delta t} C(w+dw) | 0 \rangle|^2}{\delta t^2}, \quad (3)$$

where the second term on the right hand side is an expectation value which can be sampled on a quantum computer. We encode $e^{-i\hat{H}\delta t}$ in the form of a Trotter-Suzuki decomposition [25, 26].

The optimal dw^* are determined by iteratively descending along the steepest direction given by the gradient $\frac{\partial}{\partial dw_i} L(dw, \delta t)$, starting from an initial guess dw_0 . In general, the gradient of a quantum expectation value involving parametrized quantum circuits can be determined using finite differences [38] or simultaneous perturbation techniques [39]. However, those techniques rely on an approximation of the real gradient. To improve the accuracy, we consider circuits of the general form

$$C(w) = V_p U_p(w_p) V_{p-1} \dots V_1 U_1(w_1) \quad (4)$$

where the gates V_k do not depend on any parameter and the parametrized gates $U_j(w_j)$ are of the form

$$U_j(w_j) = e^{-\frac{i}{2} w_j G_j} = \cos(w_j/2) \mathbb{I} - i \sin(w_j/2) G_j, \quad (5)$$

with $G_j^2 = \mathbb{I}$. We remark that in general G_j can be any tensor product of Pauli operators. In this case, the gradient can be computed exactly in a hardware-friendly way using the parameter shift rule [38, 40–43], obtaining

$$\begin{aligned} \frac{\partial}{\partial dw_i} L(dw, \delta t) &= \\ &= \frac{L(dw + se_i, \delta t) - L(dw - se_i, \delta t)}{2 \sin(s)}, \end{aligned} \quad (6)$$

where e_i is the versor in the i -th direction and $s \in \mathbb{R}$. We remark that our p-VQD algorithm does not require an ancilla qubit to perform measurements.

The optimisation of dw is then performed according to a standard gradient descent scheme

$$dw^{\text{new}} = dw^{\text{old}} + \eta \nabla_{dw} L(dw^{\text{old}}, \delta t), \quad (7)$$

with learning rate $\eta \in \mathbf{R}^+$. A single optimization step requires $O(p)$ measurements. The optimisation continues until the loss function goes below the desired threshold ν . Finally, once dw^* is determined, the parameters at time $t + \delta t$ are determined by

$$w(t + \delta t) = w(t) + dw^*(t) \quad (8)$$

We remark that the circuit width and depth are the same from the beginning to the end of the simulation. A sketch of the algorithm is shown in Fig 1, while an accurate study of the total hardware cost can be found in Section III.

A. Relationship with other methods

In order to understand the connection of our approach with existing methods, it is conceptually interesting to explicitly take the limit of a vanishing time step. In this limit, the parameter variation obtained with p-VQD is $dw = \dot{w}\delta t$ and \dot{w} is the solution of the equation

$$\sum_j \text{Re}[G_{kj}] \dot{w}_j = \text{Im} \left[\langle \partial_k \psi_w | H | \psi_w \rangle \right] + i \langle \psi_w | H | \psi_w \rangle \langle \partial_k \psi_w | \psi_w \rangle \quad (9)$$

where G_{kj} is the Quantum Geometric Tensor (QGT)

$$G_{kj}(w) = \left\langle \frac{\partial \psi_w}{\partial w_k}, \frac{\partial \psi_w}{\partial w_j} \right\rangle - \left\langle \frac{\partial \psi_w}{\partial w_k}, \psi_w \right\rangle \left\langle \psi_w, \frac{\partial \psi_w}{\partial w_j} \right\rangle. \quad (10)$$

This form for dw coincides with that found applying the McLachlan's variational principle [29, 32] considering also a time-dependent global phase on the ansatz state. Both McLachlan's and the time-dependent variational principle suffice to simulate real time dynamics of closed systems. Moreover, they can be shown to be equivalent under certain assumptions [29]. However, on the practical point of view, there are some differences between them due to numerical instabilities that we will analyze further in Sec. III. Defined the QGT as in Eq. (10) the TDVA relies on the evaluation of its imaginary part, which is skew-symmetric, making its inversion unstable when the off-diagonal elements are close to 0. The McLachlan's variational principle, on the contrary, requires the real part, as can be seen in Eq. (9). For this reason, it is suggested that McLachlan's is the most consistent variational principle for quantum simulation. A detailed derivation of Eq. (9) can be found in Appendix C.

III. RESULTS

To demonstrate a practical application of the p-VQD algorithm, we consider the Transverse Field Ising Model on an open chain,

$$H = J \sum_{i=0}^{N-1} \sigma_i^z \sigma_{i+1}^z + h \sum_{i=0}^N \sigma_i^x. \quad (11)$$

The first term accounts for interaction between spins while the latter represents a local and uniform magnetic field along the transverse direction x . For our simulations, we considered $J = \frac{1}{4}$ and $h = 1$. We compare the time-evolution obtained through the p-VQD against the more-established TDV-Algorithm. For both methods we consider the same circuit ansatz of the form

$$C(w) = \prod_{l=1}^d \left[\prod_{i=1}^N R_{\alpha}^{(i)}(w_{i,l}) \right] \left[\prod_{j=1}^{N-1} e^{-i w_{j,l} \sigma_j^z \sigma_{j+1}^z} \right] \quad (12)$$

where $R_{\alpha}^{(i)}(w_{i,l}) = e^{-i w_{i,l} \sigma_i^{\alpha}}$ is a single qubit rotation and α is either x or y depending whether l is odd or even, respectively. This ansatz circuit can be made deep or shallow just by varying the depth parameter d , the number of variational parameters varies accordingly. We analyzed the ideal case of a simulation in which we have access to the state vector produced by the quantum circuit (statevector simulation) and the case in which to gain information about the quantum state we have to repeatedly measure the qubits (multi-shot simulation). The two simulations coincide in the limit of infinite samples. However, when the number of samples is finite, statistical fluctuations produce a noise on the results which we will refer to as shot noise. For both statevector and multi-shot simulations we used IBM's open-source library for quantum computing, Qiskit [44].

As a first comparison, we consider the integrated infidelity $\Delta_F(T)$ achieved by both algorithms with respect to the exact simulation of the system over an entire time evolution from $t = 0$ to $t = T$. This quantity can be expressed as

$$\Delta_F(T) = \int_0^T (1 - |\langle \Psi(t) | \psi_{w(t)} \rangle|^2) dt. \quad (13)$$

We have performed several simulations both with p-VQD and the TDVA for different shots per circuit evaluation (total number of samples) and report the mean performance in Fig. 2.

At a fixed number of samples, the integrated infidelity Δ_F for the p-VQD is up to an order of magnitude below the TDVA one for the same time-step. In Appendix C it is shown that with small time-steps and in the limit

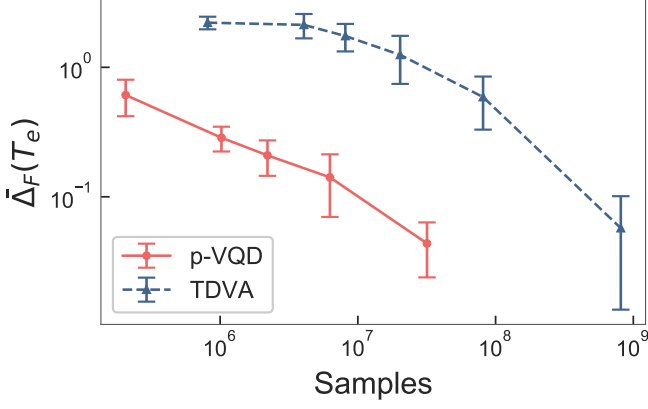


Figure 2. Mean error on fidelity accumulated over an entire time evolution for the two different methods. The plot shows, as a function of the total samples required, the fidelity error accumulated by the algorithm over an entire time evolution. The total time of evolution is $T_e = 3$ and the number of time steps is $n_{\text{steps}} = 60$ for both p-VQD and TDVA. For each number of samples the experiment has been iterated $n_{\text{iter}} = 10$ times and the data shown represent mean and standard deviation of those values.

of infinite samples (ideal measures) the parameter variation found by p-VQD coincide with the solution of the Euler-Lagrange equation generated by the McLachlan’s variational principle. The matrices of the Euler-Lagrange equations often show high condition number [45], in particular those generated by the time-dependent variational principle [29]. These ill-conditioned matrices are likely to produce large variations on the results when subject to small variations of the coefficients, as those produced by shot noise. We remark that shot noise is unavoidable for quantum computers, even for fault-tolerant devices. Improving iteratively the solution of the Euler-Lagrange equation leads to the estimate of the parameters variation, but does not require matrix inversion. As a result, we obtain a more stable algorithm against shot noise.

In Fig. 3 we compare the expectation values of the total magnetization along the \hat{x} and \hat{z} axis for the states evolved according to the two algorithms. The results are reported for a different number of measurements per circuit.

The magnetization along the \hat{x} axis proved to be the most difficult to capture for both the algorithms, suggesting that the problem could be the ansatz choice. We note that both the algorithms converge to the exact simulation values as the number of shots increases. In general, p-VQD shows comparable results with TDVA using one order of magnitude fewer shots.

To further analyze the performance of our algorithm, we studied the behaviour of the step-infidelity $L(dw, \delta t)$. In Fig. 4 we show the number of optimization steps required as a function of time and the consequent decrease of the cost function.

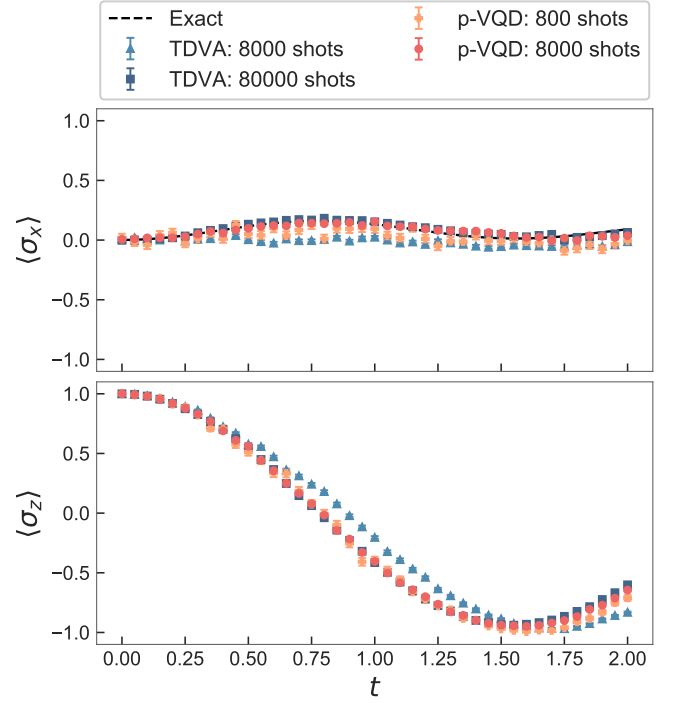


Figure 3. Total magnetization measured on simulated time evolution. The plot shows the expectation values of Pauli operators for systems simulated with p-VQD and TDVA at different shot number. We indicated the number of shots for circuit evaluation instead of total samples: 800, 8000 and 80000 shots are equivalent to $\sim 10^6, 10^7, 10^8$ total samples for the p-VQD and $\sim 10^7, 10^8, 10^9$ for the TDVA, respectively.

We remark that choosing the previous dw^* as an initial guess often leads to convergence in only one iteration. More details about the convergence of the gradient and of the step-infidelity in a single time step can be found in Appendix D.

Finally, we characterize the hardware cost of p-VQD when the number of variational parameters increases. Since the number of measures required by p-VQD scales linearly ($O(p)$) with the number of variational parameters, it has a lower asymptotic cost with respect to TDVA, which is quadratic. We can provide an accurate estimation of the hardware cost of p-VQD as an upper-bound to the total number of samples needed per simulation. We indicate with n_s and n_t the number of shots and time-steps, respectively. In the spirit of the iterative methods, we suppose that the procedure will find a solution dw^* in at most M steps. In this case, we have that the total number of hardware measurements is

$$N_{\text{samples}} \leq 2Mn_t n_s p \quad (14)$$

The number M of optimization steps depends on the ansatz, on the Hamiltonian of the system considered and on the accuracy required. For this reason we performed

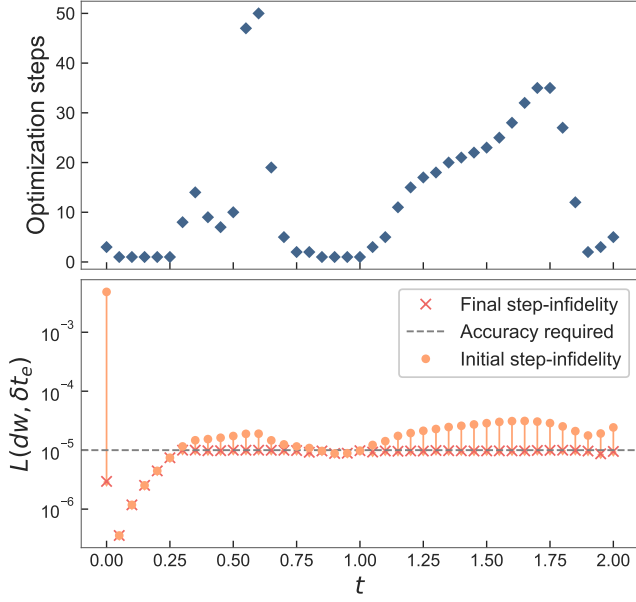


Figure 4. Number of optimization steps required (top) to decrease accuracy error per step (bottom). The algorithm optimizes the parameters shift dw until the step-infidelity $L(dw, \delta t_e)$ is below the threshold at 10^{-5} . The time step chosen is $\delta t_e = 0.05$. The analysis is performed on a statevector simulation of the system.

different simulations increasing the depth of our ansatz and reported the results in Fig 5. From the figure we deduce that $M \sim O(1)$, therefore it does not scale up by increasing the number of parameters in the ansatz circuit. Under these circumstances, the total dependence of the computational cost of the algorithm upon the number of parameters is indeed $O(p)$.

All the simulations have been done fixing a number of shots n_{shots} per circuit evaluation. For p-VQD, we made multiple simulations and then reported the mean values of our results. For TDVA the number of circuit evaluation is fixed and can be estimated a priori. This comparison does not consider the fidelities of the results obtained with the exact simulation, we know from what we showed in Fig. 2 that p-VQD has a lower error when the total number of samples is comparable with TDVA. We note that the number of samples required scales approximately linearly with the number of parameters, with fluctuations due to different optimization steps required. The lower the step-infidelity required, the higher will be the number of optimization steps, resulting in greater fluctuations on the total number of samples. In this case, we remark that more advanced methods like the use of an adaptive learning rate η can be used to improve convergence performance of p-VQD.

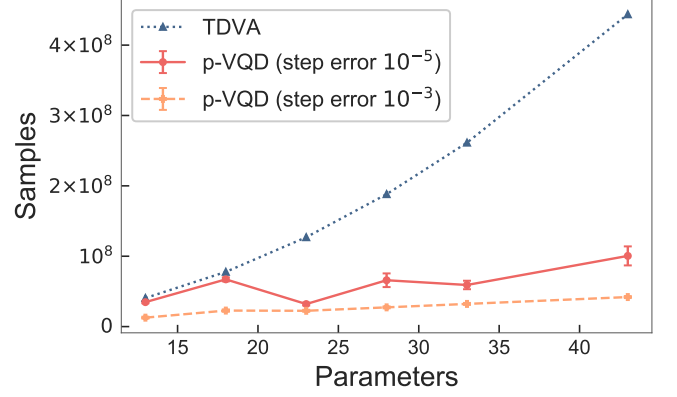


Figure 5. Measurements required as a function of circuit parameters. The plot shows the total number of circuits created and measured using p-VQD and TDVA. The number of required measurements by the TDVA is fixed, while in the p-VQD it depends on the optimization of the parameter variation. We considered $n_{\text{shots}} = 8000$ per circuit evaluation for both methods and performed multiple simulations for p-VQD, showing mean values and standard deviations of the results. Different error on the accuracy per step are showed for p-VQD.

IV. DISCUSSION

In this work, we presented a new algorithm for the efficient variational simulation of the real-time evolution of quantum systems. We have shown that it is asymptotically more hardware efficient than the standard variational algorithm, while retaining a higher accuracy. Considering the projected time evolution, we avoid numerical instabilities concerning the matrix inversion combined with statistical fluctuations due to finite shot measurements. One possible application of our approach is to study the dynamical properties of two-dimensional interacting systems, a notoriously difficult problem for classical computation. Similarly to all other variational algorithms, the choice of the right parametrization is fundamental for the algorithm to succeed. In this sense, having an efficient quantum algorithm to perform variational time evolution is essential to compare to classical results obtained with variational states either based on tensor networks [46–48], or neural networks [49, 50]. A possible improvement to further enhance the efficiency of our approach concerns the estimation of the gradient. At present, a drawback of this method is that the circuit constructed on the quantum device is approximately twice as deep as the ansatz we use to represent the system. However, by suitably controlling the number of two-qubits gates in our ansatz of choice, that represents the major source of circuit error, we believe that p-VQD is already implementable to simulate small quantum systems on available devices.

- [1] F. Arute *et al.*, *Nature* **574**, 505 (2019).
- [2] L. M. Sager, S. E. Smart, and D. A. Mazziotti, *Physical Review Research* **2** (2020), 10.1103/physrevresearch.2.043205.
- [3] P. Shor, in *Proceedings 35th Annual Symposium on Foundations of Computer Science* (IEEE Comput. Soc. Press, 1994).
- [4] D. Coppersmith, “An approximate fourier transform useful in quantum factoring,” (1994), [arXiv:quant-ph/0201067v1 \[quant-ph\]](#).
- [5] G. E. Santoro and E. Tosatti, *Journal of Physics A: Mathematical and General* **39**, R393 (2006).
- [6] I. Kassal, S. P. Jordan, P. J. Love, M. Mohseni, and A. Aspuru-Guzik, *Proceedings of the National Academy of Sciences* **105**, 18681 (2008).
- [7] I. M. Georgescu, S. Ashhab, and F. Nori, *Rev. Mod. Phys.* **86**, 153 (2014).
- [8] A. Peruzzo, J. McClean, P. Shadbolt, M.-H. Yung, X.-Q. Zhou, P. J. Love, A. Aspuru-Guzik, and J. L. O’Brien, *Nature Communications* **5** (2014), 10.1038/ncomms5213.
- [9] Y. Li and S. C. Benjamin, *Phys. Rev. X* **7**, 021050 (2017).
- [10] P. J. Ollitrault, A. Kandala, C.-F. Chen, P. K. Barkoutsos, A. Mezzacapo, M. Pistoia, S. Sheldon, S. Woerner, J. Gambetta, and I. Tavernelli, “Quantum equation of motion for computing molecular excitation energies on a noisy quantum processor,” (2019), [arXiv:1910.12890 \[quant-ph\]](#).
- [11] M. Motta, C. Sun, A. T. K. Tan, M. J. O’Rourke, E. Ye, A. J. Minnich, F. G. S. L. Brandão, and G. K.-L. Chan, *Nature Physics* **16**, 205–210 (2019).
- [12] M. Cerezo, A. Arrasmith, R. Babbush, S. C. Benjamin, S. Endo, K. Fujii, J. R. McClean, K. Mitarai, X. Yuan, L. Cincio, and P. J. Coles, “Variational quantum algorithms,” (2020), [arXiv:2012.09265 \[quant-ph\]](#).
- [13] J. Biamonte, P. Wittek, N. Pancotti, P. Rebentrost, N. Wiebe, and S. Lloyd, *Nature* **549**, 195–202 (2017).
- [14] S. E. Borujeni, S. Nannapaneni, N. H. Nguyen, E. C. Behrman, and J. E. Steck, “Quantum circuit representation of bayesian networks,” (2020), [arXiv:2004.14803 \[quant-ph\]](#).
- [15] J. Romero, J. P. Olson, and A. Aspuru-Guzik, *Quantum Science and Technology* **2**, 045001 (2017).
- [16] I. Kerenidis, J. Landman, A. Luongo, and A. Prakash, in *Advances in Neural Information Processing Systems*, Vol. 32, edited by H. Wallach, H. Larochelle, A. Beygelzimer, F. d’Alché-Buc, E. Fox, and R. Garnett (Curran Associates, Inc., 2019) pp. 4134–4144.
- [17] M. Schuld and N. Killoran, *Phys. Rev. Lett.* **122**, 040504 (2019).
- [18] M. Schuld, A. Bocharov, K. M. Svore, and N. Wiebe, *Physical Review A* **101** (2020), 10.1103/physreva.101.032308.
- [19] V. Havlíček, A. D. Córcoles, K. Temme, A. W. Harrow, A. Kandala, J. M. Chow, and J. M. Gambetta, *Nature* **567**, 209 (2019).
- [20] M. H. Amin, E. Andriyash, J. Rolfe, B. Kulchytskyy, and R. Melko, *Phys. Rev. X* **8**, 021050 (2018).
- [21] I. Cong, S. Choi, and M. D. Lukin, *Nature Physics* **15**, 1273 (2019).
- [22] P. J. J. O’Malley *et al.*, *Phys. Rev. X* **6**, 031007 (2016).
- [23] A. Kandala, A. Mezzacapo, K. Temme, M. Takita, M. Brink, J. M. Chow, and J. M. Gambetta, *Nature* **549**, 242 (2017), [arXiv:1704.05018](#).
- [24] B. Bauer, S. Bravyi, M. Motta, and G. K.-L. Chan, *Chemical Reviews* **120**, 12685 (2020).
- [25] H. F. Trotter, *Proc. Amer. Math. Soc.* **10**, 545 (1959).
- [26] M. Suzuki, *Journal of Mathematical Physics* **32**, 400 (1991), <https://doi.org/10.1063/1.529425>.
- [27] D. S. Abrams and S. Lloyd, *Phys. Rev. Lett.* **79**, 2586 (1997).
- [28] G. Ortiz, J. E. Gubernatis, E. Knill, and R. Laflamme, *Phys. Rev. A* **64**, 022319 (2001).
- [29] X. Yuan, S. Endo, Q. Zhao, Y. Li, and S. C. Benjamin, *Quantum* **3**, 191 (2019).
- [30] P. A. M. Dirac, *Mathematical Proceedings of the Cambridge Philosophical Society* **26**, 376–385 (1930).
- [31] J. Frenkel, *Wave Mechanics: Advanced General Theory* (Oxford University Press, London, 1934).
- [32] A. McLachlan, *Molecular Physics* **8**, 39 (1964).
- [33] M. Bukov, D. Sels, and A. Polkovnikov, *Phys. Rev. X* **9**, 011034 (2019).
- [34] M. Kolodrubetz, D. Sels, P. Mehta, and A. Polkovnikov, *Physics Reports* **697**, 1 (2017), geometry and non-adiabatic response in quantum and classical systems.
- [35] M. Benedetti, M. Fiorentini, and M. Lubasch, “Hardware-efficient variational quantum algorithms for time evolution,” (2020), [arXiv:2009.12361 \[quant-ph\]](#).
- [36] S.-H. Lin, R. Dilip, A. G. Green, A. Smith, and F. Pollmann, “Real- and imaginary-time evolution with compressed quantum circuits,” (2020), [arXiv:2008.10322 \[quant-ph\]](#).
- [37] J. Stokes, J. Izaac, N. Killoran, and G. Carleo, *Quantum* **4**, 269 (2020).
- [38] M. Schuld, V. Bergholm, C. Gogolin, J. Izaac, and N. Killoran, *Phys. Rev. A* **99**, 032331 (2019).
- [39] J. Spall, *Johns Hopkins Apl Technical Digest* **19**, 482 (1998).
- [40] R. M. Parrish, E. G. Hohenstein, P. L. McMahon, and T. J. Martinez, “Hybrid quantum/classical derivative theory: Analytical gradients and excited-state dynamics for the multistate contracted variational quantum eigensolver,” (2019), [arXiv:1906.08728 \[quant-ph\]](#).
- [41] G. E. Crooks, “Gradients of parameterized quantum gates using the parameter-shift rule and gate decomposition,” (2019), [arXiv:1905.13311 \[quant-ph\]](#).
- [42] A. Mari, T. R. Bromley, and N. Killoran, “Estimating the gradient and higher-order derivatives on quantum hardware,” (2020), [arXiv:2008.06517 \[quant-ph\]](#).
- [43] L. Banchi and G. E. Crooks, “Measuring analytic gradients of general quantum evolution with the stochastic parameter shift rule,” (2020), [arXiv:2005.10299 \[quant-ph\]](#).
- [44] H. A. et al., “Qiskit: An open-source framework for quantum computing,” (2019).
- [45] J. Demmel, *Numerische Mathematik* **51**, 251 (1987).
- [46] G. Vidal, *Physical Review Letters* **93**, 040502 (2004).
- [47] A. J. Daley, C. Kollath, U. Schollwöck, and G. Vidal, *Journal of Statistical Mechanics-Theory and Experiment*, P04005 (2004).
- [48] S. R. White and A. E. Feiguin, *Physical Review Letters* **93**, 076401 (2004).

[49] G. Carleo and M. Troyer, *Science* **355**, 602 (2017).

[50] M. Schmitt and M. Heyl, *Physical Review Letters* **125**, 100503 (2020), publisher: American Physical Society.

Appendix A: The projected real time evolution

We aim to simulate the evolution of a quantum system by acting on the parameters of the variational ansatz that approximates the real state of the system. The parameter variation has to satisfy Eq. (1). We are going to see how this condition can be derived defining the projected real-time evolution. Consider the projector $P_w = |\psi_w\rangle\langle\psi_w|$ and define the squared distance between the evolved parametrized state and its projection on the subspace spanned by $|\psi_{w+dw}\rangle$

$$|||\phi(\delta t)\rangle - P_{w+dw}|\phi(\delta t)\rangle||^2 \quad . \quad (\text{A1})$$

To find the best approximation for the evolved state, we want to minimize this distance finding the optimal dw . Imposing this condition we obtain

$$\begin{aligned} \arg \min_{dw \in \mathbb{R}^p} |||\phi(\delta t)\rangle - P_{w+dw}|\phi(\delta t)\rangle||^2 &= \arg \min_{dw \in \mathbb{R}^p} \left(\langle\phi(\delta t)| - \langle\phi(\delta t)|P_{w+dw} \right) \left(|\phi(\delta t)\rangle - P_{w+dw}|\phi(\delta t)\rangle \right) \\ &= \arg \min_{dw \in \mathbb{R}^p} \left[1 - 2\langle\phi(\delta t)|P_{w+dw}|\phi(\delta t)\rangle + \langle\phi(\delta t)|P_{w+dw}^2|\phi(\delta t)\rangle \right] \\ &= \arg \min_{dw \in \mathbb{R}^p} \left[1 - \langle\phi(\delta t)|P_{w+dw}|\phi(\delta t)\rangle \right] \\ &= \arg \max_{dw \in \mathbb{R}^p} |\langle\phi(\delta t)|\psi_{w+dw}\rangle|^2 \end{aligned} \quad (\text{A2})$$

where we used the idempotence property of the projector $P_{w+dw}^2 = P_{w+dw}$. With the final equivalence we see that this condition is equivalent to Eq. (1).

Appendix B: Relationship of step-infidelity with time-step and parameter variation

In this Appendix we explain the introduction of the factor $\frac{1}{\delta t^2}$ in Eq. (2). Consider the overlap contained in the step-infidelity definition in Eq. (2) and Taylor expand it in δt and dw . First, expand to the second order the time evolution operator $e^{-iH\delta t} \sim \mathbf{I} - iH\delta t - \frac{H^2}{2}(\delta t)^2$ to get

$$\begin{aligned} \langle\psi_{w+dw} | (\mathbf{I} - iH\delta t - \frac{H^2}{2}(\delta t)^2) |\psi_w\rangle \langle\psi_w | (\mathbf{I} + iH\delta t - \frac{H^2}{2}\delta t^2) |\psi_{w+dw}\rangle &= \\ = |\langle\psi_{w+dw}|\psi_w\rangle|^2 - i\delta t \langle\psi_{w+dw}|H|\psi_w\rangle \langle\psi_w|\psi_{w+dw}\rangle + i\delta t \langle\psi_{w+dw}|\psi_w\rangle \langle\psi_w|H|\psi_{w+dw}\rangle + (\delta t)^2 |\langle\psi_{w+dw}|H|\psi_w\rangle|^2 - \\ - \frac{\delta t^2}{2} \langle\psi_{w+dw}|H^2|\psi_w\rangle \langle\psi_w|\psi_{w+dw}\rangle - \frac{\delta t^2}{2} \langle\psi_{w+dw}|\psi_w\rangle \langle\psi_w|H^2|\psi_{w+dw}\rangle \end{aligned} \quad (\text{B1})$$

Now we expand to first order in dw , obtaining $|\psi_{w+dw}\rangle = |\psi_w\rangle + \sum_j dw_j |\partial_j \psi_w\rangle$. The first order contribution in δt vanishes, but also the first order contribution in dw , then we have

$$\sum_j dw_j [\langle\partial_j \psi_w|\psi_w\rangle - \langle\psi_w|\partial_j \psi_w\rangle] = 0 \quad \forall dw_j \quad (\text{B2})$$

The final result reads

$$|\langle \psi_{w+dw} | e^{-iH\delta t} | \psi_w \rangle|^2 \sim 1 + \delta t^2 \left[\sum_j \frac{dw_j}{\delta t} [2i\langle H \rangle_w \langle \partial_j \psi_w | \psi_w \rangle - 2\text{Im}[\langle \psi_w | H | \partial_j \psi_w \rangle]] - \text{Var}_w(H) + \sum_{j,k} \frac{dw_j}{\delta t} \frac{dw_k}{\delta t} \langle \partial_j \psi_w | \psi_w \rangle \langle \psi_w | \partial_k \psi_w \rangle \right] . \quad (\text{B3})$$

As $\delta t \rightarrow 0$, also $dw_j \rightarrow 0 \quad \forall j$ and their ratio remains constant. Therefore, the addition of $\frac{1}{\delta t^2}$ factor in Eq. (2) makes it independent from the time-step size in the limit of $\delta t \rightarrow 0$.

Appendix C: Equivalence between the p-VQD and the McLachlan's variational principle

In this Appendix, we show that in the limit of small time-step the parameter variation that fulfills the request in Eq. (1) is the same obtained by applying the McLachlan's variational principle [29, 32].

We start Taylor expanding the overlap to the second order: using the substitution

$$|\psi_{w+dw}\rangle = |\psi_w\rangle + \sum_k dw_k |\partial_k \psi_w\rangle + \frac{1}{2} \sum_{k,j} dw_k dw_j |\partial_k \partial_j \psi_w\rangle + o(dw^3) \quad (\text{C1})$$

we obtain

$$\begin{aligned} |\langle \phi(\delta t) | \psi_{w+dw} \rangle|^2 &= |\langle \phi(\delta t) | \psi_w \rangle|^2 + \sum_k \left[\langle \phi(\delta t) | \psi_w \rangle \langle \partial_k \psi_w | \phi(\delta t) \rangle + \langle \phi(\delta t) | \partial_k \psi_w \rangle \langle \psi_w | \phi(\delta t) \rangle \right] dw_k + \\ &+ \sum_{k,j} \left[\langle \phi(\delta t) | \partial_k \psi_w \rangle \langle \partial_j \psi_w | \phi(\delta t) \rangle + \frac{1}{2} \langle \phi(\delta t) | \partial_k \partial_j \psi_w \rangle \langle \psi_w | \phi(\delta t) \rangle + \langle \phi(\delta t) | \psi_w \rangle \langle \partial_k \partial_j \psi_w | \phi(\delta t) \rangle \right] dw_k dw_j + o(dw^3) \end{aligned} \quad (\text{C2})$$

where we used $|\phi(\delta t)\rangle = e^{-iH\delta t} |\psi_w\rangle$ as in the main text.

Then, we expand the time evolution operator to the first order $e^{-iH\delta t} = \mathbf{I} - iH\delta t + o(\delta t)$ and partially differentiate both sides of the normalization condition $||\psi_w||^2 = 1$ with respect to parameters w_i and w_j to obtain the two important properties

$$\langle \psi_w | \partial_k \psi_w \rangle = -\langle \partial_k \psi_w | \psi_w \rangle \quad (\text{C3})$$

$$\langle \psi_w | \partial_k \partial_j \psi_w \rangle + \langle \partial_k \partial_j \psi_w | \psi_w \rangle = -\langle \partial_k \psi_w | \partial_j \psi_w \rangle - \langle \partial_j \psi_w | \partial_k \psi_w \rangle . \quad (\text{C4})$$

Substituting in Eq. (C2) we have

$$\begin{aligned} |\langle \phi(\delta t) | \psi_{w+dw} \rangle|^2 &= |\langle \phi(\delta t) | \psi_w \rangle|^2 + \\ &+ i \sum_k \left[\langle \psi_w | H | \psi_w \rangle \langle \partial_k \psi_w | \psi_w \rangle - \langle \psi_w | H | \psi_w \rangle \langle \psi_w | \partial_k \psi_w \rangle + \langle \partial_k \psi_w | H | \psi_w \rangle - \langle \psi_w | H | \partial_k \psi_w \rangle \right] dw_k \delta t + \\ &+ \frac{1}{2} \sum_{k,j} \left[2\langle \psi_w | \partial_k \psi_w \rangle \langle \partial_j \psi_w | \psi_w \rangle - \langle \partial_k \psi_w | \partial_j \psi_w \rangle - \langle \partial_j \psi_w | \partial_k \psi_w \rangle \right] dw_k dw_j \end{aligned} \quad (\text{C5})$$

where we neglected the third order contribution in dw and δt . We notice that the second order term in $dw_k dw_j$ is the real part of the Quantum Geometric Tensor (QGT), as expressed in Eq. (10). Finally, in the p-VQD algorithm

we aim to find the dw that maximizes the overlap in Eq.(1), thus similarly here we impose the first order optimality condition

$$\frac{\partial}{\partial dw_k} |\langle \phi(\delta t) | \psi_{w+dw} \rangle|^2 = 0 \quad \forall k \quad (\text{C6})$$

that in the limit $\delta t \rightarrow 0$ gives the equation

$$\sum_j \text{Re}[G_{kj}] \dot{w}_j = \text{Im} \left[\langle \partial_k \psi_w | H | \psi_w \rangle \right] + i \langle \psi_w | H | \psi_w \rangle \langle \partial_k \psi_w | \psi_w \rangle \quad (\text{C7})$$

where we indicated with G the QGT, as in the main text. This is the same evolution equation for parameters w that is obtained when the McLachlan's variational principle is used to simulate real time dynamics of closed systems with pure quantum states. For an extensive review of the variational principles for time evolution of pure and mixed states, see [29].

Appendix D: Optimization routine for a single timestep

In this Appendix, we further analyze the optimization routine of our algorithm. This optimization is performed on the parameter variation dw for every time step. In this case we focus on a statevector simulation of the Transverse Field Ising Model on an open chain (see main text), considering only a single time-step (without loss of generality, the third time-step of the simulation).

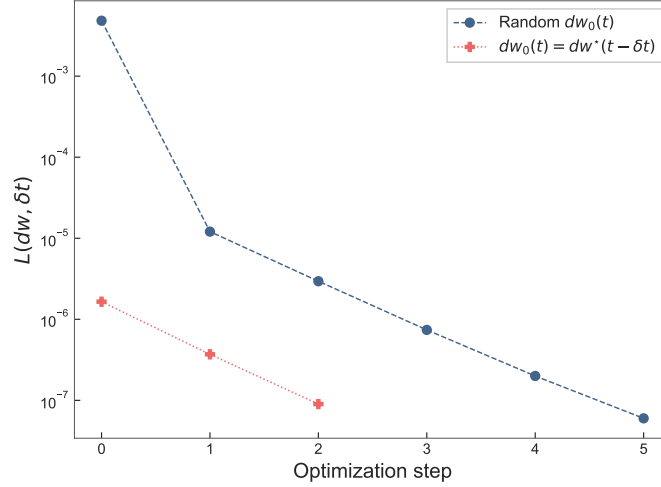


Figure 6. Infidelity as a function of the optimization step. The optimization procedure requires only a few optimization steps to greatly decrease the step-infidelity. Moreover, we compare the random choice of an initial dw_0 of order $O(\delta t)$ to the educated guess $dw_0 = dw^*(t - \delta t)$.

As Fig. 6 shows, at every optimization steps the step-infidelity is reduced of nearly a order of magnitude. The initial choice $dw_0 = dw^*(t - \delta t)$ is shown to reduce the number of steps required.

For the same optimization procedure, in Fig. 7 we show the gradient computed at each optimization step. After a few steps the absolute value of each component converges to zero, meaning that we are indeed approaching a stationary point.

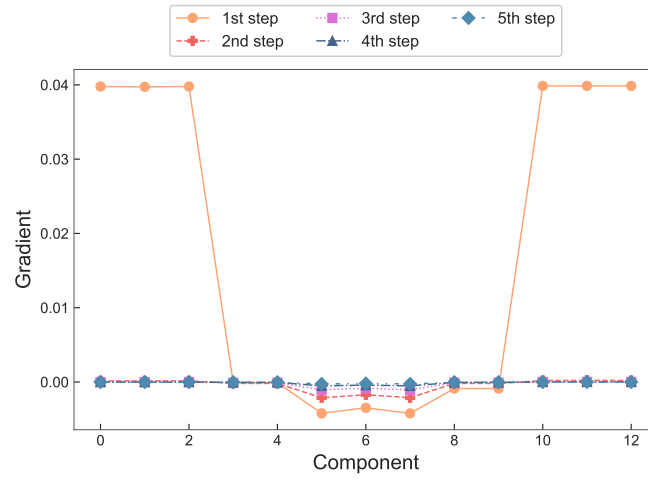


Figure 7. Gradient for each optimization step. Considering a variational ansatz with 13 parameters we show the value of each component of the gradient computed at every optimization step.